Enhancement of magnetic and electrical properties in Sc substituted BiFeO3 multiferroic

T. Durga Rao, Asmitha Kumari, Manish K. Niranjan, Saket Asthana

Advanced Functional Materials Laboratory, Department of Physics, Indian Institute of Technology Hyderabad, Hyderabad 502205, Andhra Pradesh, India

Physica B: Condensed Matter
Volume 448, 1 September 2014, Pages 267–272

http://dx.doi.org/10.1016/j.physb.2014.03.055

Enhancement of magnetic and electrical properties in Sc substituted $BiFeO_3$ multiferroic

T Durga Rao, Asmitha Kumari, Manish K. Niranjan, Saket Asthana*
Advanced Functional Materials Laboratory, Department of Physics,
Indian Institute of Technology Hyderabad, Andhra Pradesh – 502205, India
*** Author for Correspondence: asthanas@iith.ac.in**

Abstract: Polycrystalline $BiFe_{1-x}Sc_xO_3$ (x = 0, 0.05, 0.1 and 0.15) compounds are prepared using solid state reaction. The XRD patterns show that all compounds are crystallized in rhombohedral structure with *R3c* space group. An induced weak ferromagnetism in Sc substituted $BiFeO_3$ due to suppression of spiral modulated spin structure is revealed. In addition, a spin glass like behaviour is observed from the zero field cooled (ZFC) and field cooled (FC) magnetization curves in the low temperature region. Further, the coupling between the ferroelectric and (anti) ferromagnetic orders is evident from the appearance of anomaly in the dielectric data near the magnetic Néel temperature (373 ^oC). The reduction of oxygen vacancies due to Sc substitution is evident from the ac conductivity data and the

suppressed anomaly in dielectric data at 220 ^{o}C. The temperature dependence of ac conductivity is consistent with correlated barrier hopping (CBH) model. The temperature dependent ac conductivity and activation energies indicate that electronic conduction, oxygen vacancies movement and creation of defects are the prime contributors to the ac conductivity in measured temperature regions. The improved magnetic and electrical properties due to the structural modification are prominent for novel device applications.

Key words: Multiferroics, Antiferromagnetic, ac conductivity, activation energy.

1. Introduction

Multiferroic materials have become promising for technological applications due to simultaneous existence of ferroic orders such as ferroelectric, (anti)ferromagnetic and/or ferroelastic orders. Existence of coupling of ferroelectric and (anti)ferromagnetic orders imparts a great value to these materials for device applications such as actuators, data storage and sensors [1, 2]. Ferroelectricity in $BiFeO_3$ (BFO) arises due to the stereochemical activity of $6s^2$ lone pair electrons of Bi^{3+}, while the indirect magnetic exchange interaction between Fe^{3+} ions through O^{2-} causes G-type antiferromagnetic ordering. BFO is a fascinating multiferroic among all the multiferroic materials due to its high Curie temperature (T_C = 1103 K) and high Néel temperature (T_N = 643 K) [2]. However, leakage current (arises due to the presence of mixed valence states of Fe^{2+} and Fe^{3+} ions and deficiency of oxygen ions) and antiferromagnetic nature in BFO limits its potential as a material of choice for device applications. Thus the reduction of leakage current and induced ferromagnetism in BFO is highly desirable. Several attempts have been made to tackle these problems such as i) adopting various processing technique ii) cationic substitution and iii) making solid solutions. Of all these, cationic substitution is the most effective method to reduce the leakage current and to tune the multiferroic properties of BFO. Cationic substitution either at A-site or at B-site results structural distortion within the lattice which in turn modifies the physical properties of the compounds. Generally, rare earth elements such as La, Nd, Eu, Gd, Dy and Ho or II A alkaline earth metal elements like Ba, Ca, Sr etc., have been substituted at A – site [3-5] whereas transition metal elements such as Mn, Co Ti, etc., have been substituted at B – site [6, 7]. The reported experimental studies on B-site substitution are very few as compared to those at A-site. This may be primarily due to enhanced multiferroic properties obtained with A-site substitution as compared to B-site substitution. Recently, influence of Sc-in BFO has been observed in terms of variation in physical properties especially reduction in leakage current, in nano-sized particles [8] and thin films [9, 10] To the best of our knowledge, there are no reports on structural, magnetic, electrical studies in Sc substituted polycrystalline BFO compounds.

In this communication, we study structural, electric and magnetic properties of BFO with Sc substitution at the B-sites. The Sc^{3+} ion is chosen as it is more stable than Fe^{3+} ion. Since the enthalpy of Sc-O bond (681.6 ±11.3 kJ/mol) is greater than that of Fe-O bond (390.4 ±17.2 kJ/mol), it is expected that substitution of Sc for Fe could reduce the oxygen vacancies in BFO which in turn may improve electric properties by reducing the conductivity.

2. Experimental Details

Polycrystalline $BiFe_{1-x}Sc_xO_3$, (x = 0, 0.05, 0.1 and 0.15) compounds are synthesized by conventional solid-state route using high purity Bi_2O_3, Fe_2O_3 and Sc_2O_3 (purity > 99.9%) as starting materials. These powders are mixed with their stoichiometric ratios and ground thoroughly for 2 hrs. The powders are calcined in two step process at 780 °C for 2 hrs and then at 815 °C for 3 hrs. The calcined powder are pelletized in the form of circular disc of size 8 mm diameter and 1.5 mm thickness by adding freshly prepared polyvinyl alcohol (PVA) as binder in order to improve the density of the ceramics. The pellets are annealed at 450 °C for 1 hrs at the rate of 2.5 °C /min to remove binder and then finally sintered at 830°C for 3 hrs at the rate 5 °C/min. The Phase analysis of the compounds are examined by an X-ray diffractometer (Panalytical X'pert Pro) with Cu Kα radiation (λ=1.5406 Å) with a 2θ step size of 0.0167° over the angular range $20° \leq 2\theta \leq 90°$. The magnetic properties of these compounds are measured using PPMS with VSM assembly (Quantum Design, USA) up to a field of 5 Tesla. Electrical properties are measured on the silver electrode compounds using Wayne Kerr 6500B impedance analyzer with a frequency variation from 100 Hz to 1 MHz and temperature from 35 ºC to 400 ºC.

3. Results and discussion

3.1. Structural Properties

Fig. 1 shows the XRD patterns of polycrystalline $BiFe_{1-x}Sc_xO_3$ (BFSO) [x = 0 (BFO), 0.05 (BFSO5), 0.1 (BFSO10) and 0.15 (BFSO15)] compounds. Crystal structural analysis has been carried out using the Rietveld refinement using Fullprof software. A trace amount of impurity phases such as $Bi_{25}FeO_{40}$ and $Bi_2Fe_4O_9$ are observed along with the main phase. It is evident from the refinement that all the compounds crystallized in rhombohedral crystal structure with *R3c* space group. The effect of Sc^{3+} substitution in place of Fe^{3+} can be observed in terms of shift in the diffracted Bragg's peak positions towards the lower angle side in the XRD patterns. This indicates that Sc^{3+} substitution increases the lattice volume and changes the Fe-O distances and Fe-O-Fe bond angles due to its larger ionic radius (0.745 Å) than that of Fe^{3+} (0.645 Å) [10]. The structural distortion can be understood in terms of Goldschmidt tolerance factor *t*, defined as $t = (r_A + r_O)/\sqrt{2}(< r_B > + r_O)$ where $<r_B>$ is the average radius at B site and r_A and r_O are the radii of Bi^{3+} and O^{2-} respectively. The table 1 shows the lattice parameters, volume of the unit cell, and bond angle and bond distances in BFO and BSFO compounds.

3.2. Magnetic properties

In BFO, G-type antiferromagnetic ordering is superimposed with spiral modulated spin structure (SMSS) [11]. Further, the Fe^{3+} magnetic moments are coupled ferromagnetically in the pseudo cubic $(111)_c$ planes, but antiferromagnetically between the adjacent planes. The existence of a weak ferromagnetic moment is permitted by the crystal symmetry of BFO. The Fig. 2 shows magnetization (M – H) curves of BFO and BSFO compounds measured up to a maximum magnetic field of 50 kÖe at room temperature. The magnetization in BFO varies linearly with the magnetic field which indicates conventional antiferromagnetic ordering. The suppression of SMSS is evident from the appearance of weak ferromagnetism in the magnetization curves in the BSFO compounds. The remnant magnetizations M_r of BFO, BSFO5, BSFO10 and BSFO15 compounds are respectively 0.24, 0.71 and 0.33 and 1.70

memu/g. However, improvement in the magnetization is insignificant as compared to that in A-site substituted BFO compounds. Similar findings were also observed in Sc substituted BFO films [10]. Substitution of diamagnetic Sc^{3+} ion in place of Fe^{3+} ion is not only suppress SMSS, but also increases the volume of the unit cell and Fe-Fe distances. The increase in Fe-Fe bond length would weakens the magnetic exchange interaction between the Fe ions.

In order to understand the influence of Sc substitution on the magnetic ordering of BFO, zero field cooled (ZFC) and field cooled (FC) magnetization measurements are carried out from 5 K to 300 K under a magnetic field of 1000 Öe as shown in Fig. 3. Both in ZFC or FC measurements, the compounds are cooled down to 5 K from room temperature and the measurement has been carried under warming conditions. The Sc substituted BFO compounds also exhibit magnetic behavior similar to that in BFO. The magnetization decreases as the temperature is decreased from 300 K and shows thermomagnetic irreversibility between ZFC and FC curves at 170 K. Similar behavior has been observed in nanosized particles [8], single crystal [12] , and polycrystalline ceramics [13]. The splitting between ZFC and FC magnetization curves is attributed to spin glass like behavior [8, 12] in these compounds. As the temperature is further decreased below 160 K, the two magnetization curves again merge at low temperature. The temperature variation of magnetization (5-300 K) shows i) its basic antiferromagnetic nature from 300 K to 100 K and ii) An increase in magnetization with decrease of temperature especially in the low temperature below 25 K. The sharp increase in magnetization below 25 K reveals that the development of incommensurate magnetic structure in all the compounds [14].

3.3. Dielectric and electrical properties

Fig. 4 shows the frequency variation of dielctric constant (ε_r) and loss tangent ($\tan\delta$) at the room temperature for BFO and BSFO compounds. The high value of ε_r in the low frequency region is due to various polarization contributions such as interfacial, dipolar, ionic and electronic. The value of ε_r decreases up to 10 kHz and becomes frequency independent with the increase of frequency. The loss tangent value decreases from 0.013 (for BFO) to 0.004 (BSFO15) at 10 kHz. Generally, conductivity in BFO arises due to the hopping of charge carriers between Fe^{2+} and Fe^{3+}. Reduction in loss tangent value with the substitution of Sc indicates the reduction in Fe^{2+} ions which further reduces the conductivity and loss values [10].

Fig. 5 shows the temperature dependence of dielectric constant (ε_r) and loss tangent (tanδ) for BFO and Sc substituted BFO compounds at different temperatures. The dielectric constant shows almost temperature independent behavior up to 300 ^oC and then increases sharply in all compounds. An anomaly is observed around 350 ^oC near antiferromagnetic to paramagnetic transition and a slight frequency dependence of dielectric maxima towards higher temperature side with the increase of applied frequency. These anomalies well accounted with the thermodynamic theory of multiferroics where ferromagnetic order and ferroelectric order coexist [15]. An appearance of endothermic peak from our differential scanning calorimetry study and drop in magnetization from temperature dependence of magnetization data at 373 ^oC for BFO (not shown here) confirm the magnetic phase transition. This dielectric anomaly near 350 ^oC signifies the disappearance of magnetic ordering within the long range ferroelectrically ordered stable phase. In the vicinity of Néel

temperature, there exist significant changes in the lattice parameters without affecting the rhombohedral structure [16]. Schmidt et al [17] have reported the following criteria for occurrence of intrinsic magneto-electric coupling (MEC); i) a change or an anomaly in the temperature dependence of dielectric constant in the close proximity of magnetic transition, ii) changes in dielectric constant in the presence of magnetic field. Although magneto-dielectric and magnetic field dependence of electric polarization studies presumably may evolve better insight about MEC effects, however, appearance of an anomaly in temperature dependent dielectric constant near about T_N (as confirmed from our magnetic and DSC studies) can be concluded the presence of MEC [18-20].

As the space charge polarization (which arises due to the presence of oxygen vacancies, defects, etc.,) in BFO is thermally activated, the loss tangent values shoots up at high temperature or near the magnetic Néel temperature. As shown in Fig. 6, a small dielectric anomaly has been observed near 220 ^oC in the dielectric constant data which is consistent with other reported works [21, 22]. The anomaly can also be seen in the loss tangent data at the same temperature. The anomaly at 220 ^oC is attributed to the transient interaction between oxygen ions vacancies and Fe^{2+} and Fe^{3+} redox [21, 22]. The oxygen vacancies and Fe^{2+} ions are formed during the synthesis of the compounds at high temperature at longer times. These oxygen vacancies and Fe^{2+} ions are responsible for the conductivity in the compound. The effect of Sc substitution clearly reflects in the dielectric behavior of BFO. The Sc substitution decreases the oxygen vacancies which in turn causes stability of Fe^{2+} / Fe^{3+} couple-oxygen vacancies interactions. Hence the peak around 220 ^oC which is highly prominent in BFO gets suppressed with the Sc substitution [18].

3.4. A.C conductivity studies

The ac electrical conductivity was calculated by using the relation,

$$\sigma_{ac} = \varepsilon_o \varepsilon_r \omega \tan\delta \qquad [1]$$

Where ε_o is permittivity of free space and ω is the angular frequency. Fig. 7 shows the frequency dependence of ac conductivity at different temperatures. The ac conductivity shows the dispersion in the low frequency region and nearly converges in high frequency region for all compounds. The frequency dependence of ac conductivity at room temperature obeys the universal power law

$$\sigma_{ac} = A\omega^S \qquad [2]$$

Above room temperature, this dependence follows the equation [23]

$$\sigma_{ac} = A_1\omega^{S_1} + A_2\omega^{S_2} \qquad [3]$$

Where A, A_1 and A_2 are temperature dependent parameters and s, s_1 and s_2 are both temperature and frequency dependent parameters. The values of s_1 and s_2 are determined by the slopes of the curves drawn between $\ln\sigma_{ac}$ and $\ln\omega$ in the low and high frequency regions respectively. The s_1 decreases as the temperature increases and eventually approaches to zero at high temperature. As the temperature increases, conductivity can be described by Joncher's power law [24]:

$$\sigma_{a.c} = \sigma(0) + A\omega^s \qquad [4]$$

Where $\sigma(0)$ is the dc conductivity, *A* is the temperature dependent factor and *s* is an exponent. The frequency dependence part is generally explained on the basis of two mechanisms. In the case of Quantum Mechanical Tunneling (QMT) through the barrier separating the two localized sites, the ac conductivity follows linear temperature dependence. The exponent *s* is independent of temperature but slightly decreases with frequency according to the given formula [25]

$$s = 1 - \frac{4}{\ln(1/\omega\tau_o)} \quad [5]$$

In the case of Correlated Barrier Hopping (CBH), *s* decreases with the increase of temperature [26] and is given by following relation,

$$s = 1 - \frac{6kT}{W_M + kT\ln(\omega\tau_o)} \quad [6]$$

Where W_M is the maximum energy barrier, ω is angular frequency and τ_o is the characteristic relaxation time of the charge carrier. It is observed that for BFO and BSFO compounds, *s* values decrease with temperature. Our experimental results are consistent with the CBH model and the conduction process is thermally activated. The decrease in ac conductivity in Sc substituted can be accounted as follows. The Sc^{3+} ion is a diamagnetic with completely vacant 3*d* orbital in its outermost orbit and consequently its energy is lower than Fe^{3+} ion. In other words, Sc^{3+} ion is more stable than Fe^{3+}. The conductivity, depends on number of charge carriers and their mobility and, is given by following relation

$$\sigma = ne\mu \quad [7]$$

The substitution of Sc^{3+} at Fe^{3+} ion will reduces oxygen vacancies which in turn reduce the number of Fe^{2+} ions. The decrease in the number of oxygen vacancies and charge carriers hopping from Fe^{2+} to Fe^{3+} ions leads to reduction in conductivity in the substituted compounds which is consisted with the dielectric data.

Fig. 8 shows the Arrhenius plots of ac conductivity of BFO and BSFO compounds at 100 kHz. The ac conductivity increases with the increase of temperature and follows the Arrhenius equation

$$\sigma_{a.c} = \sigma_o \exp(-E/kT) \quad [8]$$

Where *k* is the Boltzmann constant and *E* is the activation energy. The activation energy is calculated by taking the linear fit to the curve drawn between $\ln\sigma_{ac}$ and *1000/T*. The compounds show activation energies around 0.2 eV below 120 ^oC (region I) and 0.7 eV from 120 ^oC to 230 ^oC (region II) and 1-1.4 eV above 230 ^oC (region III). The very low activation energies in region I are attributed to electron hopping conduction. In region II, contribution of short range of oxygen vacancies to the conductivity is expected. In region III, conductivity is attributed due to long range movement of oxygen vacancies or creation of defects [27, 28].

4. Conclusions

The polycrystalline $BiSc_xFe_{1-x}O_3$ (x = 0, 0.05, 0.1and 0.15) compounds are synthesized by conventional solid-state route. Compounds are crystallized in rhombohedral structure with *R3c* (IUCr No. 161) space group. Enhancement in the magnetization in Sc substitution compounds is due to the induced weak ferromagnetism which is attributed to the lattice distortion with the Sc substitution. The coupling between the ferroelectric and (anti) ferromagnetic orders is evidenced from the appearance of anomaly in dielectric loss tangent

data near the magnetic Néel temperature (373 ^{o}C). However, studies on the effect of magnetic field on dielectric constant and electric polarization are under progress, which may evolve the better understanding of magneto-electric coupling. Sc substitution reduces the ac conductivity by reducing oxygen vacancies and Fe^{2+} number in $BiFeO_3$. The ac conductivity follows universal power law and the transport mechanism of charge carries follows correlated barrier hopping (CBH). The activation energies calculated from Arrhenius plot revealed that electronic hopping, oxygen vacancies movement and creation of defects are the contributors to the ac conductivity.

ACKNOWLEDGEMENT

Authors are grateful to the Department of Science and Technology (DST), India for their financial support under Fast Track scheme (SR/FTP/PS–065/2011) to carry out this work.

REFERENCES

[1] M.J. Fiebig, Phys. D 38 (2005) R123.
[2] N. Hur, S. Park, P.A. Sharma, Nature 429 (2004) 392.
[3] V.A. Khomchenko, D.A. Kiselev, J.M. Vieira, L. Jian, A.L. Kholkin, A.M.L. Lopes, Y.G. Pogorelov, J. P. Araujo, M. Maglione, J. Appl. Phys. 103 (2008) 024105.
[4] T. Durga Rao, T. Karthik, Saket Asthana, J Rare Earths 31 No. 4 (2013) 370.
[5] T. Durga Rao, T. Karthik, Adiraj Srinivas, Saket Asthana, Solid State Comm. 152 (2012) 2071.
[6] F. Chang, N. Zhang, F. Yang, J. Phys. D: Appl. Phys. 40 (2007) 7799.
[7] I. Sosnowska, W. Schäfer, W. Kockelmann, Appl. Phys. A 74 [Suppl.] (2002) S1040.
[8] D.P. Dutta, B.P. Mandal, R. Naik, G. Lawes, A.K. Tyagi, J. Phys. Chem. C 117 (2013) 2382.
[9] S.R. Shannigrahi, A. Huang, N. Chandrasekhar, D. Tripathy, A.O. Adeyeye, Appl. Phys. Lett. 90 (2007) 022901.
[10] S.R. Shannigrahi, A. Huang, D. Tripathy, A.O. Adeyeye, J. Magn. Magn. Mater. 320 (2008) 2215.
[11] I. Sosnowska, T Peterlin-Neumaier, E. Steichele, J. Phys. C 15 (1982) 4835.
[12] M.K. Singh, W. Prellier, M.P. Singh, R.S. Katiyar, J.F. Scott, Phys. Rev. B 77 (2008) 144403.
[13] Y.J. Zhang, H.G. Zhang, J.H. Yin, H.W. Zhang, J.L. Chen, W.Q. Wang, G.H. Wu, J. Magn. Magn. Mater. 322 (2010) 2251.
[14] Z.P. Chen, C. Wang, T. Li, J.H. Hao, J.C. Zhang, J Supercond Nov Magn. 23 (2010) 527.
[15] V.R. Palkar, J. John, and R. Pinto, Appl. Phys. Lett. 80 (2002) 1628.
[16] S. Goswami, D. Bhattacharya, P. Choudhury, B. Ouladdiaf, T. Chatterji, Appl. Phys. Lett. 99 (2011) 073106.
[17] R. Schmidt, J. Ventura, E. Langenberg, N.M. Nemes, C. Munuera, M. Varela, M.G. Hernandez, C. Leon, J. Santamaria, Phys. Rev. B 86 (2012) 035113.
[18] P. Uniyala, K.L. Yadav, J. Alloys and Compd. 511 (2012) 149.
[19] P. Pandit, S. Satapathy, P.K. Gupta, V.G. Sathe, J. Appl. Phys. 106 (2009) 114105.
[20] G.L. Yuan, S. Wing, J. Appl. Phys. 100 (2006) 024109.
[21] M. Polomska, W. Kaczmerk, Z. Pajak, Phys. Status Solidia 23 (1974) 567.
[22] R.K. Mishra, D.K. Pradhan, R.N.P. Choudhary, A. Banerjee, J. Phys.: Condens. Matter 20 (2008) 045218.
[23] K. Funke, Prog. Solid State Chem. 22 (1993) 111.
[24] A.K. Jonscher, Nature 267 (1977) 673.
[25] A. Ghosh, Phys. Rev. B 47 (1993) 23.
[26] G.E. Pike, Phys. Rev. B 6 (1972) 4.
[27] P. Pandit, S. Satapathy P.K. Gupta, Physica B: Condensed Matter 406 (2011) 2669.
[28] J.C. Chenand, J.M. Wu, Appl. Phys. Lett. 91 (2007) 182903.

Figures captions

Fig. 1. XRD patterns of BFO and BSFO compounds. The asterisk ∗ and ♦ represent impurity phases corresponding to $Bi_{25}FeO_{40}$ and $Bi_2Fe_4O_9$ respectively.

Fig. 2. Magnetization hysteresis loops of BFO and BSFO compounds at 300 K. The inset shows the enlarged view of magnetization data near origin.

Fig. 3. Temperature dependence of magnetization of (a) BFO, (b) BSFO5, (c) BSFO10 and (d) BSFO15 compounds under the magnetic field of 1000 Öe.

Fig. 4. Frequency variation of dielctric constant (ε_r) at the room temperature for BFO and BSFO compounds. The inset shows the frequency variation of loss tangent ($\tan\delta$).

Fig. 5. Temperature variation of dielectric constant(ε_r) and loss tangent (tanδ) of BFO and BSFO compounds at different frequencies.

Fig. 6. Temperature variation of (a) dielectric constant ε_r and (b) loss tangent tanδ of BFO and BSFO compounds around the 220 ^oC.

Fig. 7. Frequency variation of ac conductivity of (a) BFO, (b) BSFO5, (c) BSFO10 and (d) BSFO15 compounds at different temperatures.

Fig. 8. Temperature dependence of ac conductivity of BFO and BSFO compounds at different frequencies.

Table captions

Table 1. Lattice parameters, volume of the unit cell, bond angle and bond distance of BFO and BSFO compounds.

Figures:

Figure – 1

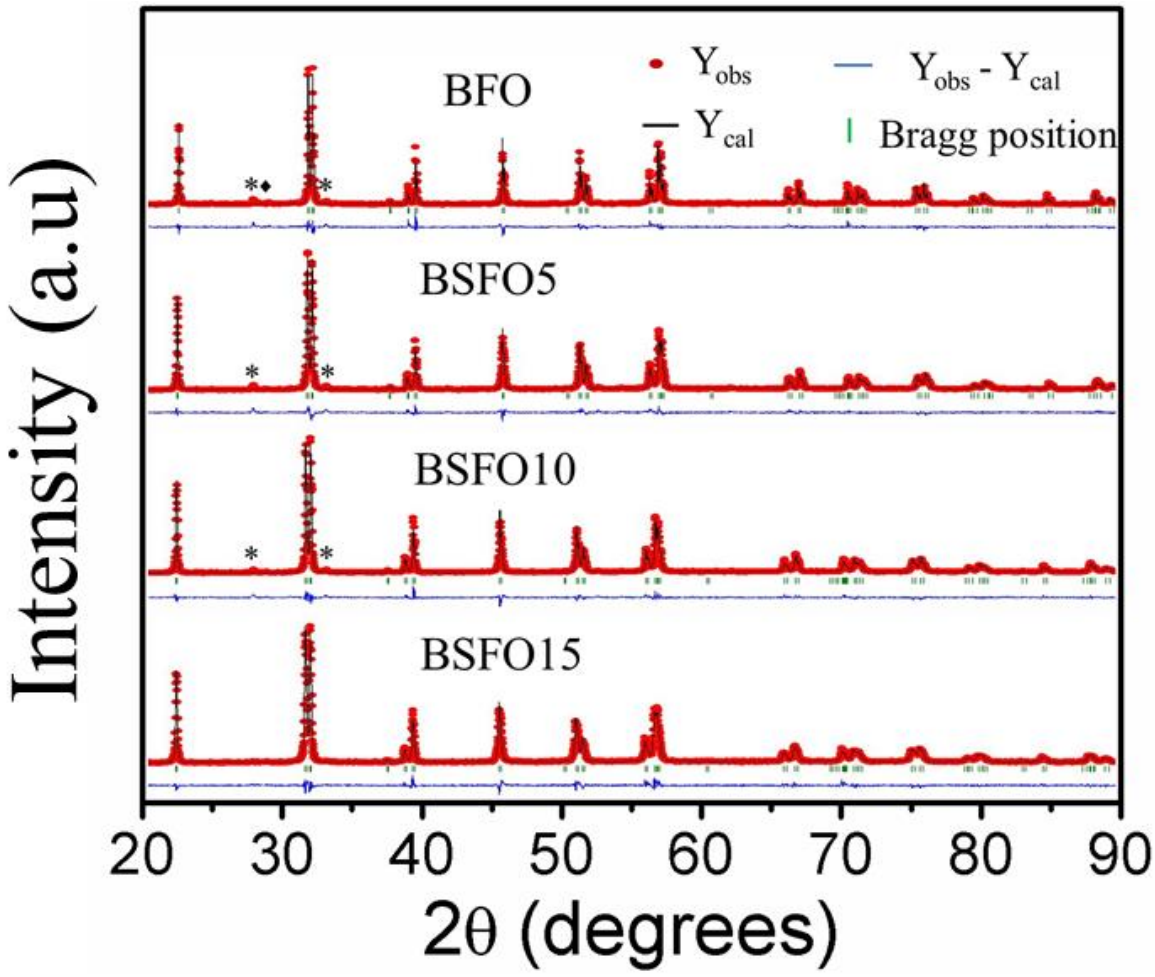

Figure – 2

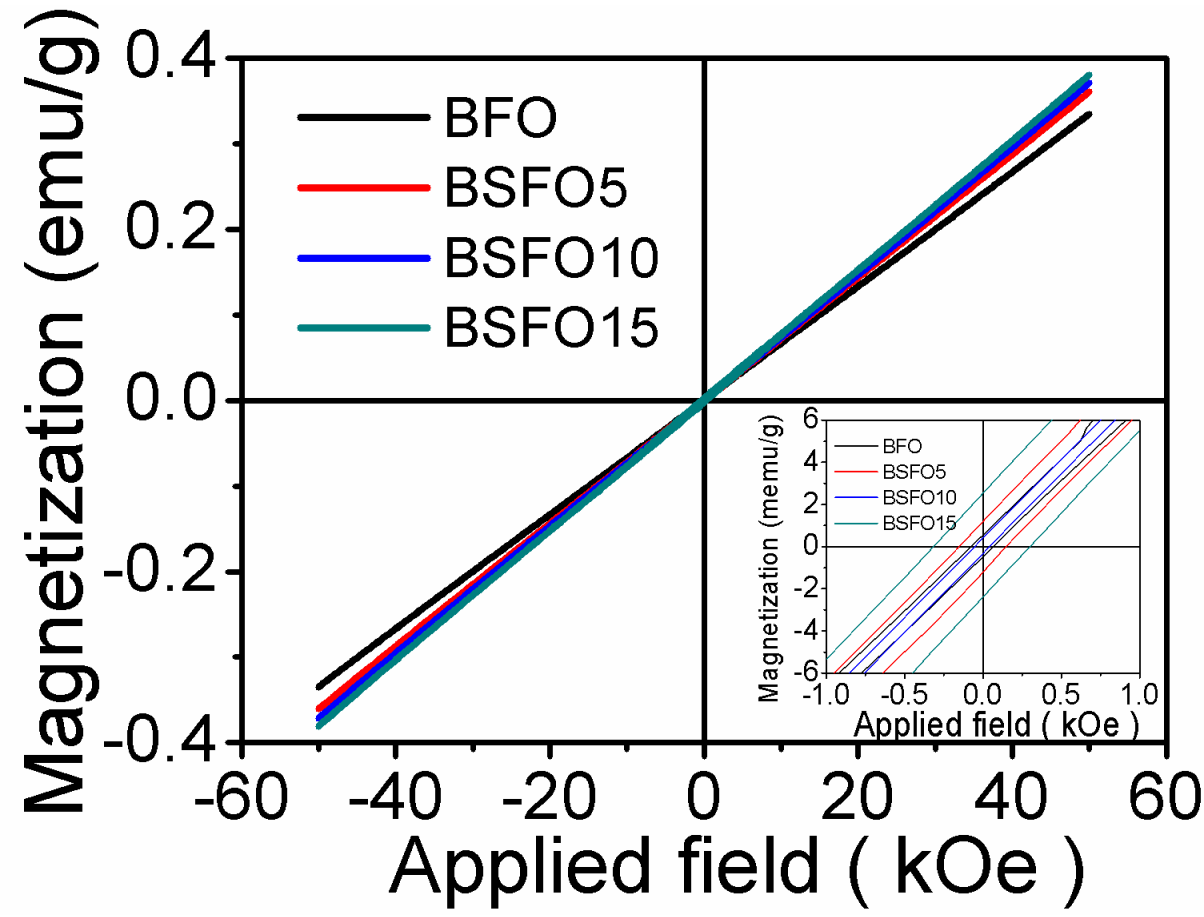

Figure – 3

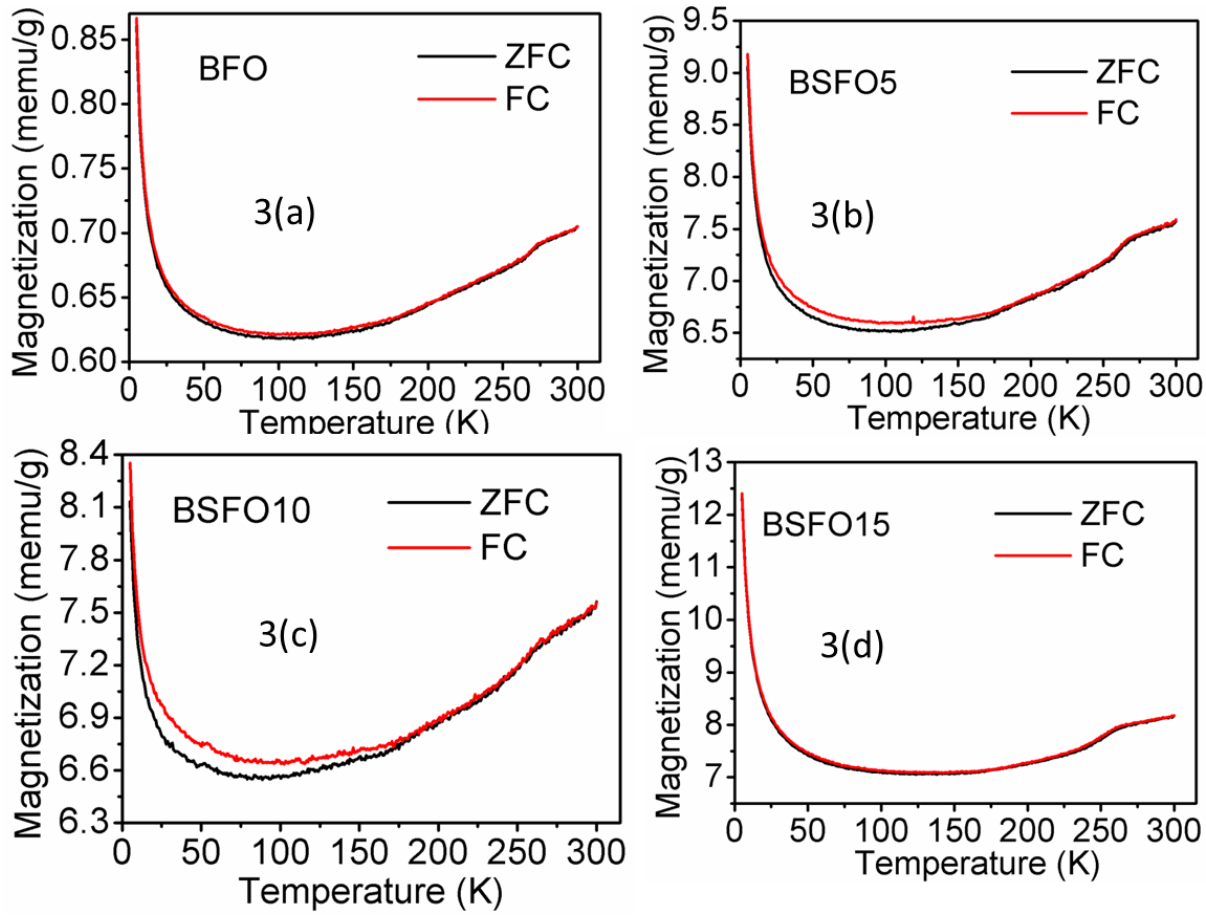
BFO
ZFC
FC
3(a)
Magnetization (memu/g)
Temperature (K)
BSFO5
ZFC
FC
3(b)
Magnetization (memu/g)
Temperature (K)
BSFO10
ZFC
FC
3(c)
Magnetization (memu/g)
Temperature (K)
BSFO15
ZFC
FC
3(d)
Magnetization (memu/g)
Temperature (K)

Figure – 4

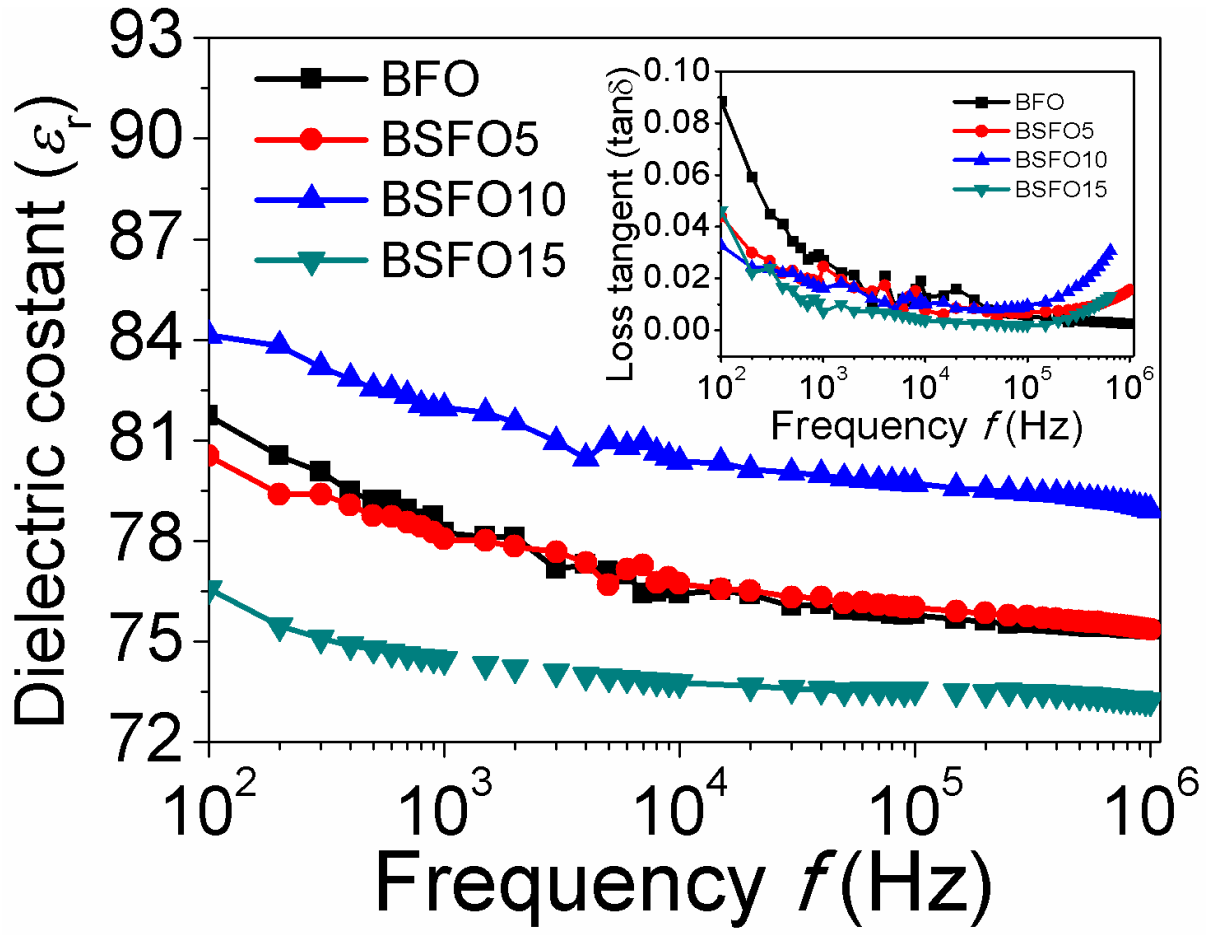
Dielectric costant (ε_r)
93
90
87
84
81
78
75
72
10^2
10^3
10^4
10^5
10^6
Frequency f(Hz)
BFO
BSFO5
BSFO10
BSFO15
Loss tangent (tanδ)
0.10
0.08
0.06
0.04
0.02
0.00
Frequency f(Hz)

Figure – 5

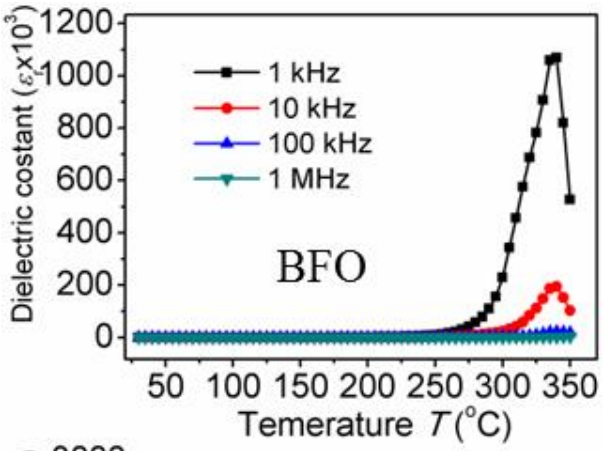
Dielectric costant (ε_rx10^3)
1 kHz
10 kHz
100 kHz
1 MHz
BFO
Temerature T(°C)

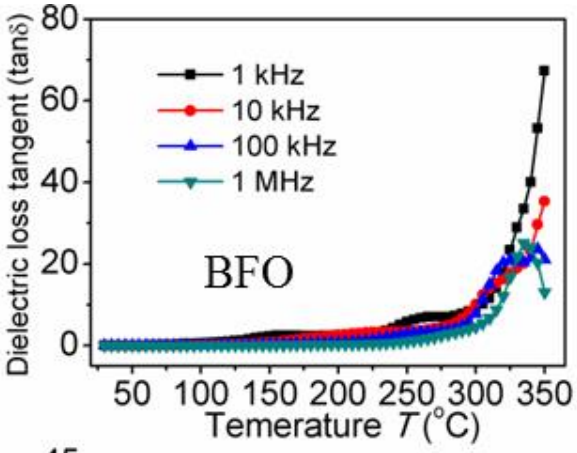
Dielectric loss tangent (tanδ)
1 kHz
10 kHz
100 kHz
1 MHz
BFO
Temerature T(°C)

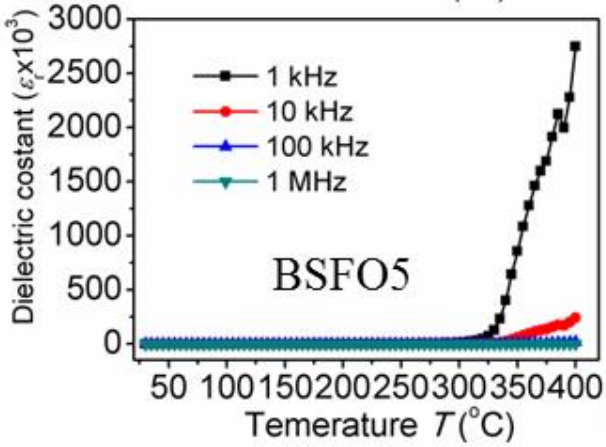
Dielectric costant (ε_rx10^3)
1 kHz
10 kHz
100 kHz
1 MHz
BSFO5
Temerature T(°C)

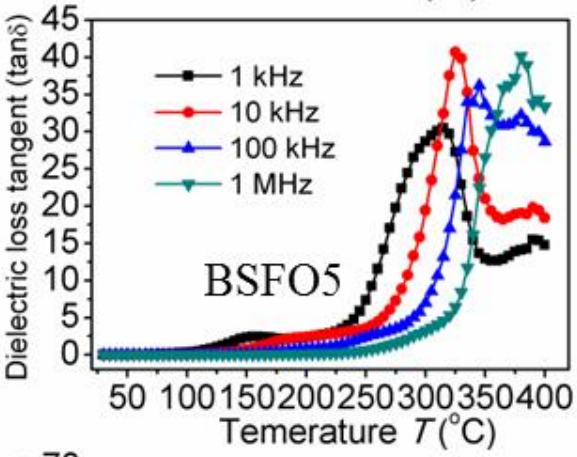
Dielectric loss tangent (tanδ)
1 kHz
10 kHz
100 kHz
1 MHz
BSFO5
Temerature T(°C)

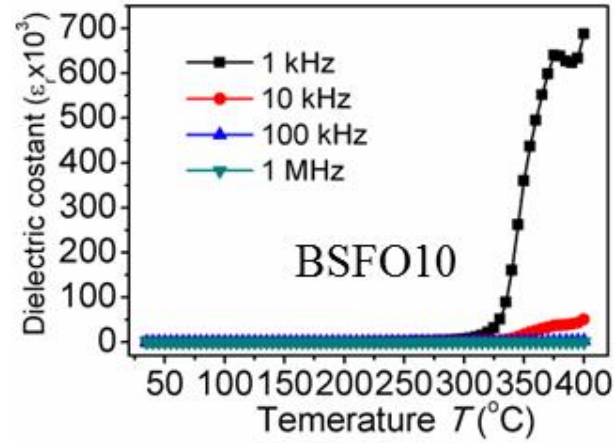
Dielectric costant (ε_rx10^3)
1 kHz
10 kHz
100 kHz
1 MHz
BSFO10
Temerature T(°C)

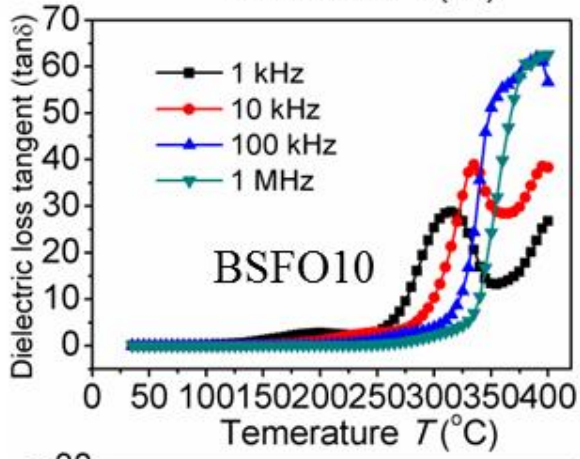
Dielectric loss tangent (tanδ)
1 kHz
10 kHz
100 kHz
1 MHz
BSFO10
Temerature T(°C)

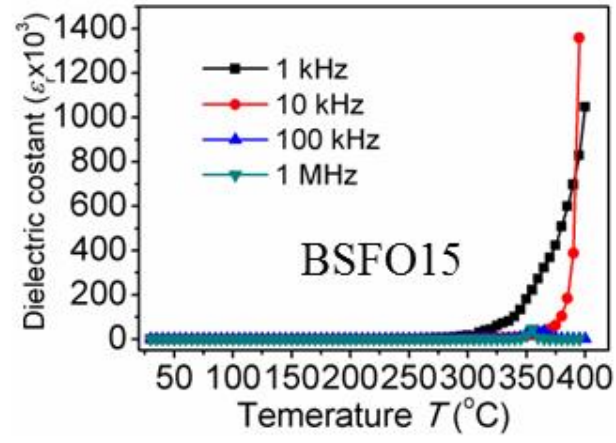
Dielectric costant (ε_rx10^3)
1 kHz
10 kHz
100 kHz
1 MHz
BSFO15
Temerature T(°C)

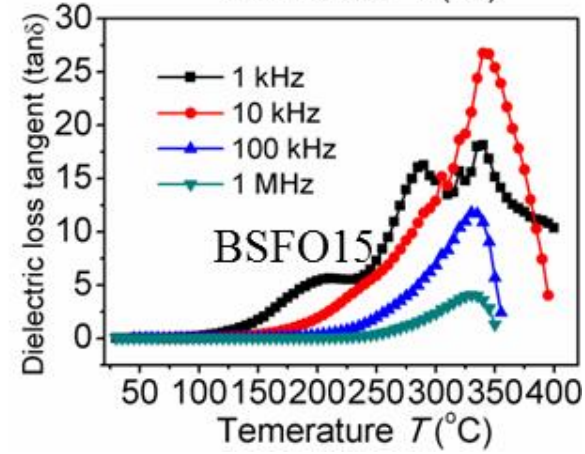
Dielectric loss tangent (tanδ)
1 kHz
10 kHz
100 kHz
1 MHz
BSFO15
Temerature T(°C)

Figure – 6

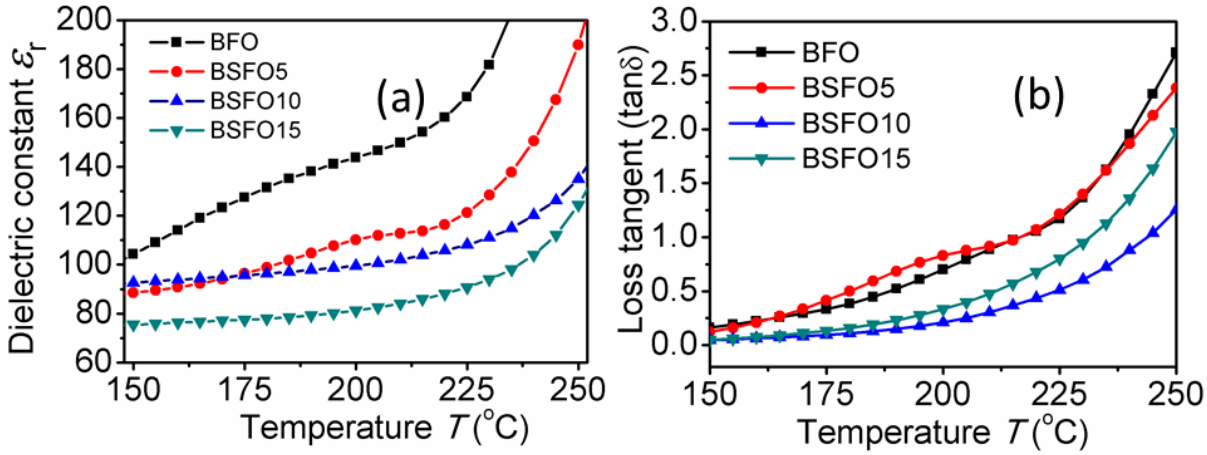

Figure – 7

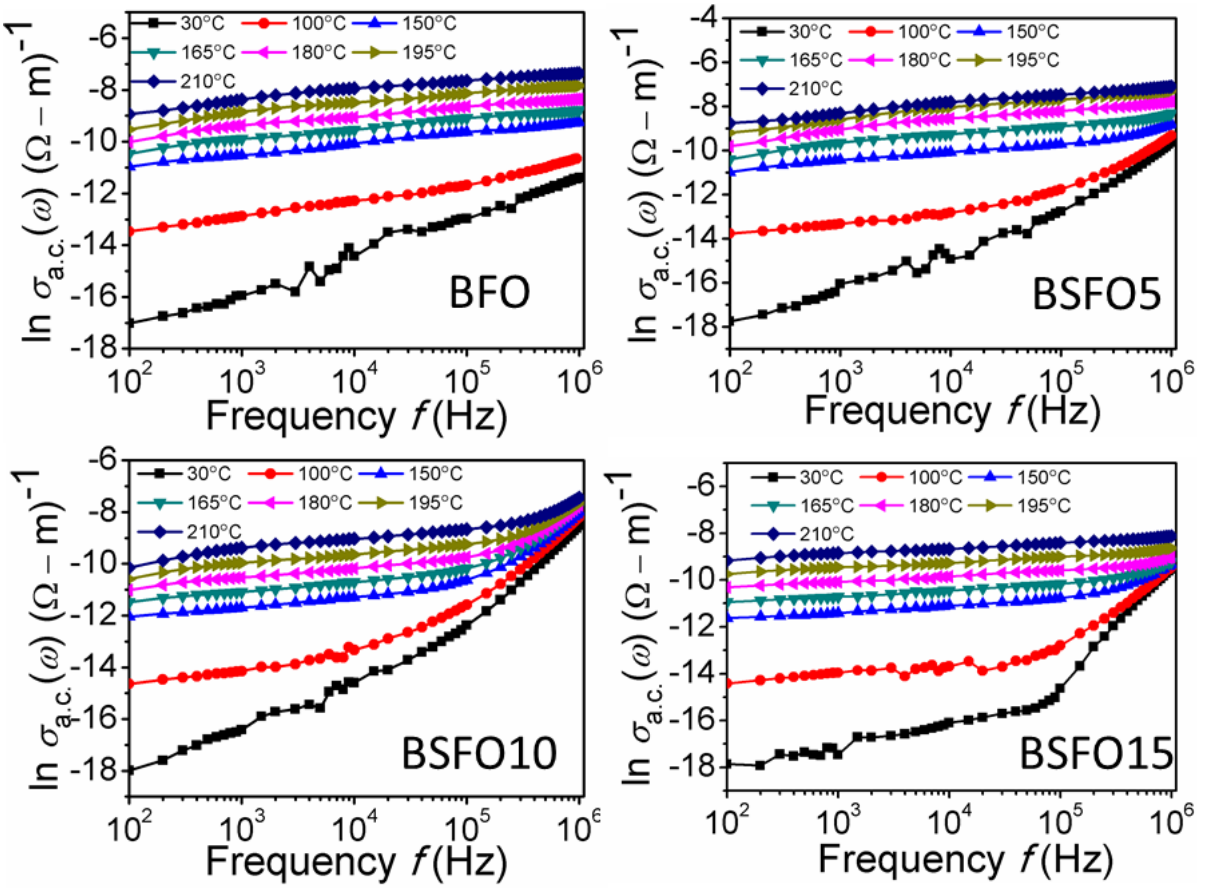

Figure – 8

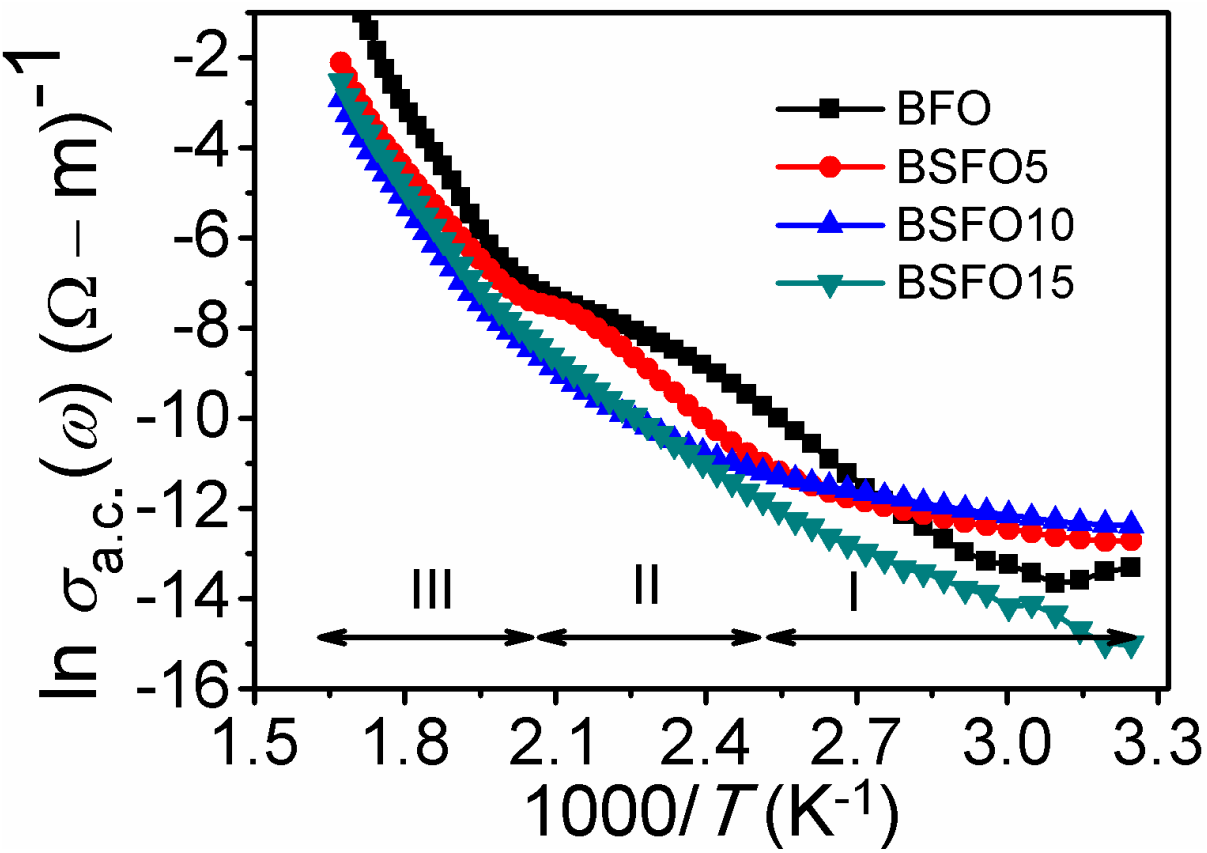
BFO
BSFO5
BSFO10
BSFO15
III
II
I
ln σa.c. (ω) (Ω – m)-1
1000/ T (K-1)
-2
-4
-6
-8
-10
-12
-14
-16
1.5
1.8
2.1
2.4
2.7
3.0
3.3